Coherent laser cooling with trains of ultrashort laser pulses

J. Malamant [1], N. Gusakova,[2,3] H. Sandaker [1], I. T. Sorokina [2], D. Comparat [4], and A. Camper [1,*]

[1]*Department of Physics, University of Oslo, Sem Saelandsvei 24, 0371 Oslo, Norway*
[2]*Department of Physics, NTNU, Norwegian University of Science and Technology, Trondheim 7491, Norway*
[3]*Physics Department, CERN, 1211 Geneva 23, Switzerland*
[4]*Laboratoire Aimé Cotton, Université Paris-Saclay, CNRS, 91405 Orsay, France*

We propose to extend coherent laser cooling from narrowband to broadband transitions by using trains of ultrashort broadband pulses. We analytically study two possible methods to reduce the momentum spread of a distribution by several units of photon momentum in a single spontaneous emission lifetime. We report on numerical simulations of one-dimensional laser cooling of a two-level system with realistic parameters. With this scheme, coherent laser cooling can in particular be implemented in the case of fast species with a short lifetime such as positronium.

I. INTRODUCTION

Laser cooling is a well-established technique to increase the phase-space density of an ensemble of particles [1,2]. It is based on the interplay of two processes. Internal-state laser excitation is used to reduce the particles' momentum spread without changing entropy. Then, spontaneous emission dissipates entropy such that the number of particles with low momentum and in the same internal state increases. For a momentum distribution of N internal level particles which are initially all in the ground state, the maximum of the position-momentum phase-space density can at most be increased by a factor N without dissipating entropy by populating all N levels within the same elementary part of the position-momentum space [3]. The time it takes to compress the momentum spread depends on the ability of the laser to move the particles with high absolute momentum from the ground state to one of the $(N-1)$ available excited states with low absolute momentum in a time short in front of the shortest spontaneous emission lifetime of all excited states.

For species prone to annihilation (such as positronium [4,5], the bound state of an electron and a positron), radioactive decay, photoionization, or molecular dissociation, interaction with the cooling laser is limited in time by the fast disintegration of the system. For those that are also usually produced in rather small amounts compared to stable elements, a technique allowing one to cool the whole momentum distribution is highly desirable. Recently, the development of *coherent laser cooling* techniques [6,7] demonstrated that it is possible to hasten the process of laser cooling. In a way similar to stimulated focusing and the deflection of atomic beams [8], these techniques make use of a succession of absorption and stimulated emission to compress the momentum spread in an accelerated way compared to standard Doppler laser cooling. Coherent laser cooling has been designed for

narrow line transitions and is currently restricted to narrow momentum distributions by the use of modulated narrowband lasers. Here, we propose to extend coherent laser cooling to broad line transitions and large Doppler profiles by using trains of ultrashort broadband pulses to drive the process. We discuss two different methods to manipulate the momentum distribution and reduce its rms in the one-dimensional case. The first approach consists of moving the positive- and negative-momentum halves of the Doppler profile towards zero momentum. The second approach is designed to transform the initial Maxwell-Boltzmann distribution into another Maxwell-Boltzmann distribution with half the initial momentum rms. For both methods, we derive the analytical formula predicting the evolution of the momentum rms as a function of the number of pulses in the train in the case of ideal population transfer. We further test the robustness of one of the approaches by performing numerical simulations for a series of trains of pulses interacting with a Maxwell-Boltzmann distribution using parameters achievable with today's laser technology and including various realistic effects such as nonideal population transfer, spontaneous emission, and photoionization from the excited states.

II. IDENTICAL-PULSES METHOD

In this section, we first consider an ideal case based on an $N = 2$ level system with an arbitrary one-dimensional distribution ρ_0 describing the initial momentum population of atoms in the ground state. First, we consider the *identical pulses* method, which, after an initial desymmetrization step, consists of swapping the populations in the ground and excited states across the entire momentum distribution to compress the momentum rms of the distribution as much as possible (see Fig. 1). The population transport can be realized with a series of identical pulses after desymmetrization. This is the main strength of this method, and we therefore refer to it as *identical pulses*. Typically, $\rho_0(n)$ is a Maxwell-Boltzmann distribution sampled on integer multiples of $\hbar k$ (one unit of
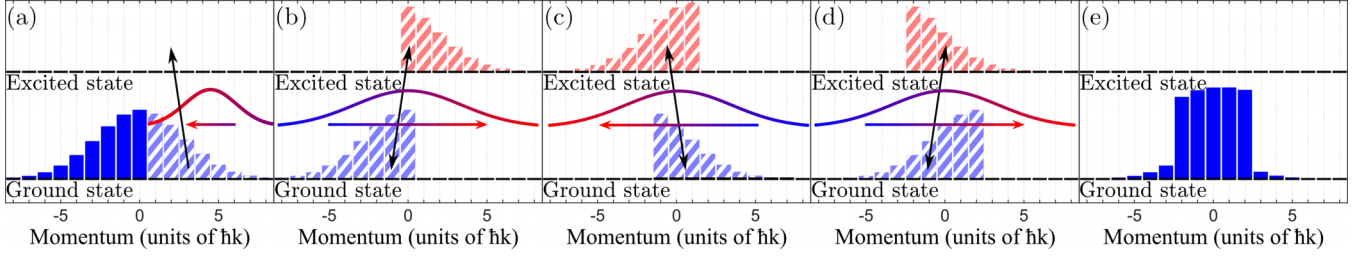

FIG. 1. Illustration of coherent laser cooling with identical pulses on a distribution with an initial momentum rms of $\simeq 5\hbar k$. Colors reflect the electronic internal level. Blue (red) corresponds to the ground (excited) state. (a) Initial distribution. [(b)–(d)] Distributions corresponding to $M = 1$ to $M = 3$ in Eq. (1), respectively. (e) Distribution after relaxation via spontaneous emission. The color gradient in the Gaussian shapes represents the laser frequency chirp of pulses that could be used for this type of adiabatic population transfer. The arrow under the Gaussian shapes represent the direction of propagation of the laser pulses. The black arrows indicate the direction of population transfer.

photon momentum), but the derivations reported in this paper are general and apply to any type of distribution.

The system is initially in the ground state, and we consider ideal population transfer for all pulses in the train. As a first step, we assume that the total duration of the train is negligible in front of the spontaneous emission lifetime of the excited state τ_{SE} and therefore assume no transfer of population by spontaneous emission. In the train, the first pulse (or desymmetrization pulse) is particular and is shaped to transfer only half of the momentum distribution [see Fig. 1(a)] from the ground to the excited state and remove $1\hbar k$ from all particles with strictly positive momentum ($n > 0$) by absorption. The second pulse in the train propagates in the direction opposite to the first one and interacts with the whole momentum distribution. The particles with negative or null momentum are transferred from the ground to the excited state and gain $1\hbar k$ from absorption, while the particles that were in the excited state lose $1\hbar k$ from stimulated emission and end up in the ground state. A train of pulses with an alternating direction of propagation is then used to interact with the whole distribution and repeat the population transfer towards the lower class of velocities. Next, we derive the analytical formula predicting the evolution of the momentum spread as a function of the number of pulses for the scheme we just described.

To describe the most general case, we introduce $\rho_1(n)$, the initial distribution of momentum for atoms in the excited state, so $\sum_n[\rho_0(n) + \rho_1(n)] = 1$. Being in the *wrong* initial state, the evolution of the $\rho_1(n)$ momentum is opposite to that of the particles in the *right* initial state $\rho_0(n)$. The evolution of the momentum rms $p_{rms}(M)$ (in units of $\hbar k$) with the number of pulses in the train M can be expressed for $M \geqslant 1$ as

$$p_{rms}^2(M) = \sum_{n \leqslant 0}[n + (M - 1)]^2 \rho_0(n) + \sum_{n > 0}(n - M)^2 \rho_0(n)$$
$$+ \sum_{n \leqslant 0}[n - (M - 1)]^2 \rho_1(n) + \sum_{n > 0}(n + M)^2 \rho_1(n).$$
$$(1)$$

Equation (1) corresponds to a hyperbolic behavior with a minimum $p_{rms,m}$ reached for $M_m = \lfloor M_{mc} + \frac{1}{2} \rfloor$ pulses:

$$p_{rms,m} = \sqrt{p_{rms,0}^2 + M_m(M_m - 2M_{mc}) + M_{ms}}. \quad (2)$$

The momentum rms of the initial distribution $p_{rms,0}$, M_{mc}, and M_{ms} are given in Appendix. For symmetrical momentum

distributions, we note that $M_{ms} = M_{mc}$. Equation (2) is very general and can be used for any discrete momentum distribution to evaluate how fast and by how much the standard deviation of a distribution can be reduced under the ideal conditions assumed to derive it. We note that, in the absence of spontaneous emission, the entropy of the system is unchanged throughout the laser-particle interaction. In the case of an initial Maxwell-Boltzmann distribution of atoms all in the ground state, it is possible to show that

$$\lim_{p_{rms,0} \to \infty} \frac{p_{rms,0}}{p_{rms,m}} = \frac{1}{\sqrt{1 - \frac{2}{\pi}}} \simeq 1.66. \quad (3)$$

For high enough initial spreads, a momentum-spread compression factor close to 1.66 can be reached with this technique using a train made of $\simeq p_{rms,0}\sqrt{\frac{2}{\pi}}$ pulses.

The hyperbolic shape of $p_{rms}(M)$ and the existence of an absolute minimum are intrinsic to the specific way the different parts of the distribution are manipulated with the identical pulses. In particular, the ground-state particles with the smallest initial absolute momentum see their momentum increase in absolute value. As a result, the momentum-spread compression $\frac{p_{rms,0}}{p_{rms,m}}$ is smaller than the optimal factor of 2 allowed for two-level systems [3].

III. OPTIMAL-TRANSPORT METHOD

In order to approach the factor of 2 in momentum-spread compression predicted by theory for a two-level system, we introduce a second method in which only the outermost parts of the momentum distribution are translated towards its center at each step in order to keep a Gaussian shape for the momentum distribution (see Fig. 2). This method is inspired by the linear rearrangement solution to the Monge-Kantorovich problem consisting of finding the optimal transport function dividing the rms of a Maxwell-Boltzmann distribution by a factor of 2 with a linear cost function. We therefore refer to it as the *optimal transport* method. The general idea is to use pairs of counterpropagating pulses which do not interact with classes of momentum in which both internal states are populated. In a pair of counterpropagating pulses, the two pulses are almost identical. Two consecutive pairs of pulses are, however, different. The first pair of pulses transfers the atoms with momentum larger than $1\hbar k$ or smaller than $-2\hbar k$
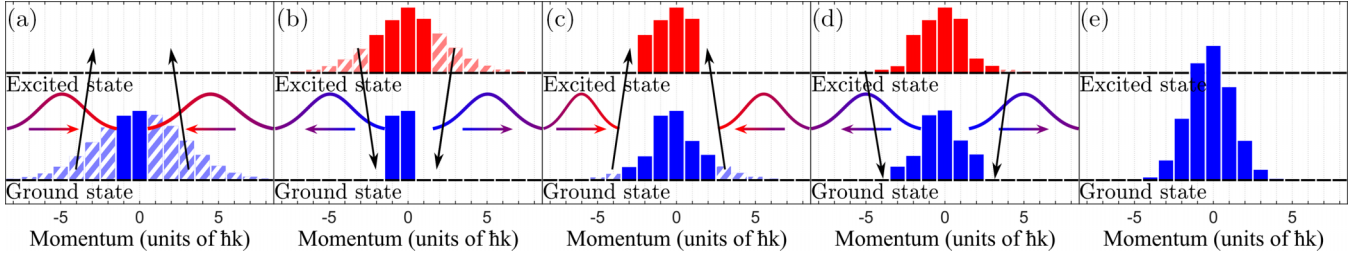
FIG. 2. Illustration of coherent laser cooling with optimal transport on a distribution with an initial momentum rms of $\simeq 5\hbar k$. Colors reflect the electronic internal level. Blue (red) corresponds to the ground (excited) state. (a) Initial distribution. Distributions corresponding to (b) $M = 1$, (c) $M = 2$, and (d) $M = 3$ in Eq. (4). (e) Distribution after relaxation via spontaneous emission.

from the ground to the excited state with a reduction in the absolute momentum of $1\hbar k$. The next pair of pulses transfers the atoms with momentum larger than $2\hbar k$ or smaller than $-3\hbar k$ from the excited to the ground state, again removing $1\hbar k$ from the absolute momentum of all particles, and so on. In this case, the evolution of the momentum spread with the number of pulses can be expressed for $M \geqslant 1$ as

$$
\tilde{p}_{\mathrm{rms}}^2(M) = \sum_{n=-M+1}^{M-1} n^2[\rho_0(2n) + \rho_0(2n+1)]
$$
$$
+ \sum_{n \geqslant M} n^2[\rho_0(n+M) + \rho_1(n-M)]
$$
$$
+ \sum_{n \leqslant -M} n^2[\rho_0(n-M+1) + \rho_1(n+M-1)].
$$
(4)

For $\rho_1(n) = 0$, $\tilde{p}_{\mathrm{rms}}(M)$ is monotonically decreasing (see Fig. 3), and

$$
\lim_{M \to \infty} \tilde{p}_{\mathrm{rms}}(M) = \sqrt{\frac{\tilde{p}_{\mathrm{rms},0}^2}{4} - \sum_{-\infty, n \text{ odd}}^{\infty} \frac{2n-1}{4}\rho_0(2n+1)}.
$$

For a number of pulses M (see Fig. 2) large compared to the initial momentum rms, the momentum compression factor is very close to 2. For an initial distribution such that $\forall\, n \in \mathbf{Z}$, $\rho_0(2n+1) = 0$, the theoretical minimum $\frac{\tilde{p}_{\mathrm{rms},0}}{2}$ is reached. The use of optimal transport allows us to reach higher momentum-spread compression factors at the cost of a more complicated population manipulation. The optimal number of pulses in optimal transport is a compromise between the level of momentum-spread compression and the total length of the train, which should still be short compared to the relaxation-time constant of the system.

In Fig. 2(e), the momentum distribution is slightly asymmetric. This is due to the discretization of the momentum space on integers of $\hbar k$. If, instead, the momentum space is discretized on the half-integer multiples of $\hbar k$, optimal transport can be composed of pairs of exactly identical pulses addressing classes of momentum larger than $1.5\hbar k$, $2.5\hbar k$, and so on. In this case, the final distribution is perfectly symmetric.

IV. MULTIPLE TRAINS OF SHORT PULSES

So far, we have discussed the evolution of the momentum distribution as a function of the number of pulses (one panel in Figs. 1 and 2) in a single train (all panels in Figs. 1 and 2). We

will now discuss the possibility to use several trains of pulses to further reduce the momentum spread of the distribution. After a train with an optimal number of pulses has interacted with the ensemble of particles, the system starts to relax to the ground state. Once all atoms are back to the ground state, it is possible to send a second train of pulses and further reduce the momentum spread. The relaxation to ground state through spontaneous emission can be modeled as an exponential decay with a certain probability to gain or lose at most $1\hbar k$. Starting from $\rho_0(n)$ and $\rho_1(n)$, exponential decay after time τ is simulated by replacing $\rho_0(n)$ and $\rho_1(n)$ with [10]

$$
\bar{\rho}_0(n, \tau) = \rho_0(n) + 0.2\rho_1(n-1)e^{-\tau/\tau_{\mathrm{SE}}}
$$
$$
+ 0.6\rho_1(n)e^{-\tau/\tau_{\mathrm{SE}}}
$$
$$
+ 0.2\rho_1(n+1)e^{-\tau/\tau_{\mathrm{SE}}}
$$
$$
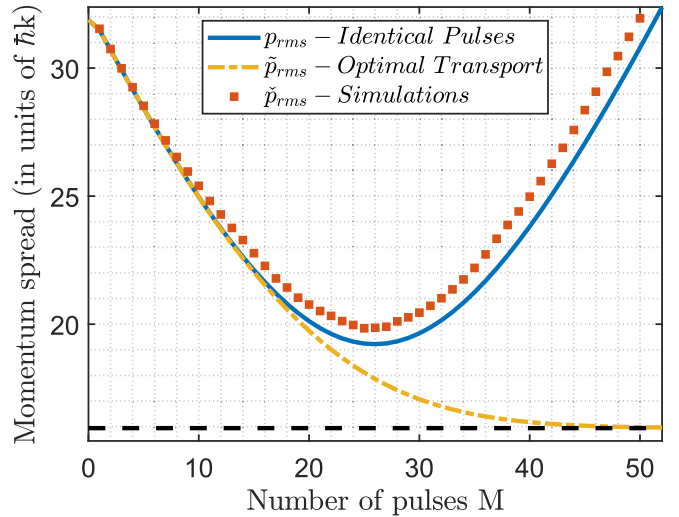\bar{\rho}_1(n, \tau) = \rho_1(n)(1 - e^{-\tau/\tau_{\mathrm{SE}}}).
$$

FIG. 3. Evolution of the momentum rms as a function of the number of pulses as predicted analytically for the identical-pulses [p_{rms}, see Eq. (1); solid blue line] and optimal-transport [$\tilde{p}_{\mathrm{rms}}$, see Eq. (4); yellow dot-dashed line] methods and as simulated numerically for identical pulses including modeling of the laser, spontaneous emission, photoionization, and annihilation [$\check{p}_{\mathrm{rms}}$, see Eq. (10); red squares]. The initial standard deviation of the Maxwell-Boltzmann distribution is $p_{\mathrm{rms},0} = 31.88\hbar k$ (corresponding to 300 K for positronium [11]). The black dashed horizontal line features the $p_{\mathrm{rms},0}/2$ level.
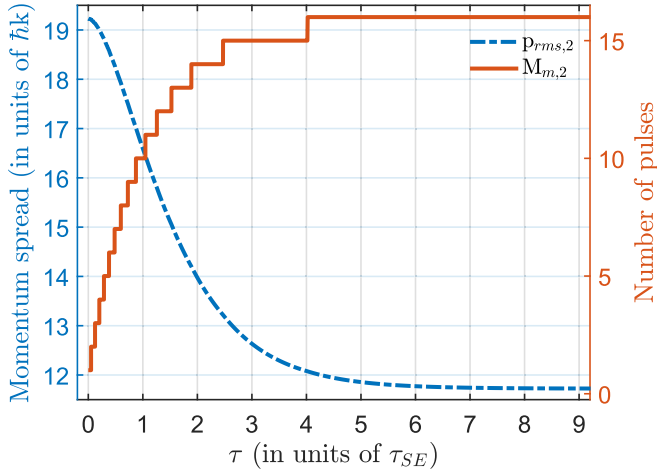
FIG. 4. Optimization of the delay τ between the first and second trains of identical pulses (dot-dashed blue line). Minimum standard deviation $p_{\mathrm{rms},2}$ (see Sec. IV) achievable at the end of a second train of $M_{m,2}$ pulses (solid red line) as a function of the delay τ between the first and second trains of identical pulses. $p_{\mathrm{rms},2}(\tau = 0) = p_{\mathrm{rms},1} = 19.23\hbar k$ is the minimum value reached after a first train of identical pulses with $M_{m,1}$ pulses (see Fig. 3).

A good order of magnitude for the time interval between two consecutive trains of pulses is τ_{SE}. However, after one exponential decay time, about 37% of the atoms initially in the excited state will still be excited. Being in the wrong initial state, these particles will be warmed up instead of cooled down by the second train of pulses.

To study the influence of the delay τ between two consecutive trains of identical pulses, we introduce spontaneous emission and compute the momentum spread after two trains of identical pulses for each value of τ. The momentum rms $p_{\mathrm{rms},2}$ at the end of the second train with $M_{m,2}$ pulses is computed with Eq. (2) applied to $\bar{\rho}_0(n, \tau)$ and $\bar{\rho}_1(n, \tau)$. As an example, we start from a Maxwell-Boltzmann distribution with $p_{\mathrm{rms},0} = 31.88\hbar k$ with all atoms in the ground state; the first train is made of $M_{m,1} = 26$ pulses after desymmetrization, yielding a minimum momentum rms $p_{\mathrm{rms},1} = 19.23\hbar k$ (see Fig. 3). The optimal number of pulses in the second train $M_{m,2}$ after desymmetrization depends on τ. The result for the identical pulses is presented in Fig. 4. $p_{\mathrm{rms},2}$ is the momentum rms reached at the end of the second train of pulses. When τ increases, there is more time for atoms in the excited state to relax to the ground state. As a result, when the second train starts, fewer atoms are in the wrong state, and $p_{\mathrm{rms},2}$ continuously decreases as a function of τ. Figure 4 suggests that a value of $\tau \simeq 4\,\tau_{\mathrm{SE}}$ is a good compromise between shortening the process as much as possible and reaching the lowest possible rms at the end of the second train of pulses. For $\tau = 4\tau_{\mathrm{SE}}$, the highest number of pulses in the second train is reached, and the momentum rms after the second train of pulses is less than $1\hbar k$ away from the value that would be reached for an infinitely long delay between the two trains. Considering that with the first train of pulses, the rms dropped from $31.88\hbar k$ to $19.23\hbar k$, if $\tau = 4\tau_{\mathrm{SE}}$, $12.65\hbar k$ are removed in $4\tau_{\mathrm{SE}}$, which is a factor of 6 higher than what can be achieved with traditional laser cooling. Considering a reduction of the

momentum rms by approximately $7\hbar k$ with the second train, if the delay between the second and third trains of pulses is still $4\tau_{\mathrm{SE}}$, a total reduction of $20\hbar k$ is achieved in $8\tau_{\mathrm{SE}}$. For momentum distributions with a larger initial spread, the gain would be even larger.

The number of pulses $M_{m,i}$ decreases with the train index i and is different in each train, as is expected from Eq. (2) considering that the momentum spread at the beginning of the ith train decreases with i. This is a novelty in comparison to previously introduced coherent laser-cooling mechanisms [7] in which cycles of identical sweep and wait periods were proposed, with one sweep consisting of one excitation and one stimulated-emission event. In this sense, the technique we propose here tests the limits of efficiency of coherent laser cooling.

By comparison with traditional Doppler cooling, this result sheds light on the limit of efficiency of coherent laser cooling with trains of ultrashort laser pulses. Indeed, traditional Doppler cooling allows one to reduce the momentum spread by $1\hbar k$ in $2\tau_{\mathrm{SE}}$ at best. If the reduction in momentum spread that would occur is smaller than this rate, the proposed coherent-cooling scheme is no longer competitive and should not be used. In the case of two- and three-dimensional cooling, it is advisable to change the direction of cooling after this limit is reached. For large enough initial momentum spreads, the schemes proposed here remain very competitive in comparison with classical two- and three-dimensional Doppler cooling even when a waiting period of $4\tau_{\mathrm{SE}}$ between each dimension is observed.

Concerning the identical pulses, we note that the use of a desymmetrization step can be avoided in the case of a pulsed source of atoms for which it is reasonable to assume a spatial distribution of momentum such that the particles with the highest absolute momentum are farthest from the spatial center of the ensemble. In this situation, the same momentum rms reduction is obtained by using pairs of identical pulses synchronized to reach the center of the ensemble of particles at the same time, in a fashion reminiscent of SWAP cooling [7]. In this situation, there is no need to manipulate classes of momentum with $\hbar k$ resolution. As for optimal transport, in the particular case of positronium, the frequency shift associated with a momentum change of $1\hbar k$ amounts to $\simeq 6.15$ GHz. As demonstrated with cutting-edge setups [12,13], it is possible to perform pulse shaping with the required resolution on a 1-THz large spectral bandwidth.

In the next section, we report on numerical simulations of the identical pulses, including a realistic description of the laser, spontaneous emission, and photoionization from the excited state.

V. NUMERICAL SIMULATIONS

We use the Quantum Toolbox in Python (QUTIP) to simulate the evolution of the ensemble of atoms. The behavior of the $\hat{\rho}$ density operator is described as an open quantum system using the Lindblad master equation [14]:

$$\frac{d\hat{\rho}}{dt} = [\hat{H}, \hat{\rho}] + \sum_i \left(\hat{L}_i \hat{\rho} \hat{L}_i^\dagger - \frac{1}{2}\{\hat{L}_i^\dagger \hat{L}_i, \hat{\rho}\} \right). \quad (5)$$

The unitary part of the transformation is described by Hamiltonians in the momentum space ($\mathcal{H}_V$) and internal state space ($\mathcal{H}_I$), which compose the Hamiltonian $\hat{H} = \hat{H}_I \otimes \hat{H}_V$. Additionally, the dissipative behavior is modeled with Lindblad operators $\hat{L}_i$ with corresponding coupling strengths Γ_i. In $\hat{H}_I$, we put the atomic levels $|g\rangle$ and $|e\rangle$. The one-dimensional momentum space is discrete and sampled on multiple integers of $1\hbar k$. In this situation, spontaneous emission can be properly described by redistributing the decaying excited states to the ground state with three different momenta as described previously [10]. This discrete momentum space allows us to properly describe the dynamics of the system for a rms width large compared to $\hbar k$. The inclusion of sub-Doppler effects would, however, require using a higher sampling rate of this space. Furthermore, the Hamiltonian is transformed into the rotating frame and is written as

$$
\hat{H} = \hbar \sum_{n=-n_{\text{bin}}}^{n_{\text{bin}}} [n^2 \omega_{\text{rec}} |g, n\rangle \langle g, n| + (\omega_0 - \omega_L(t) + n^2 \omega_{\text{rec}})
$$
$$
\times |e, n\rangle \langle e, n| - \Omega(t)|g, n\rangle \langle e, n \pm 1|
$$
$$
- \Omega(t)|e, n \pm 1\rangle \langle g, n|], \tag{6}
$$

where $\Omega(t) = \frac{dE(t)}{\hbar}$ is the instantaneous Rabi frequency, $E(t)$ is the laser field envelope, d is the dipole moment of the transition, and ω_0 is the resonant angular frequency of the transition. The instantaneous angular laser frequency is given by $\omega_L(t)$, and $\omega_{\text{rec}} = \frac{\hbar k^2}{2m}$ is the laser recoil frequency. Two (dead) states $|\text{ph}\rangle$ and $|\text{ann}\rangle$ can be added to $\hat{H}_I$ to take into account losses such as photoionization (ph) and annihilation (ann). These effects as well as spontaneous emission are included like in other works in the literature [7,11] using the following Lindblad operators:

$$
\hat{L}_{\text{SE}} = \sqrt{\Gamma_{\text{SE}}} \sum_{n=-n_{\text{bin}}+1}^{n_{\text{bin}}-1} (\sqrt{0.6}|g, n\rangle \langle e, n|
$$
$$
+ \sqrt{0.2}|g, n-1\rangle \langle e, n| + \sqrt{0.2}|g, n+1\rangle \langle e, n|), \tag{7}
$$

$$
\hat{L}_{\text{ph}} = \sqrt{\Gamma_{ph.}} \sum_{n=-n_{\text{bin}}}^{n_{\text{bin}}} |\text{ph}, n\rangle \langle e, n|, \tag{8}
$$

$$
\hat{L}_{\text{ann}} = \sqrt{\Gamma_{\text{ann}}} \sum_{n=-n_{\text{bin}}}^{n_{\text{bin}}} |\text{ann}, n\rangle \langle g, n|. \tag{9}
$$

In our simulations, ω_{rec} was set to zero to limit computing time. This approximation has a negligible impact on the results. In the following, we present results in the case of positronium for which $|g\rangle = |1S\rangle$ and $|e\rangle = |2P\rangle$. $\Gamma_{\text{ph}} = \sigma_{\text{ph}} \frac{I(t)}{\hbar \omega_0}$ is the photoionization rate and is related to the photoionization cross section $\sigma_{\text{ph}} = 2.6 \times 10^{-22}\,\text{m}^2$, $I(t)$ is the laser intensity, $\Gamma_{\text{ann}} = \frac{1}{142\,\text{ns}}$ is the annihilation rate in the $|1S\rangle$ state, and $\Gamma_{\text{SE}} = \frac{1}{3.2\,\text{ns}}$ is the spontaneous emission rate.

The momentum spread $\check{p}_{\text{rms}}$ is quantified by the standard deviation of the velocity distribution. In our studies, $\check{p}_{\text{rms}}$ refers to the standard deviation of only the ground and excited states:

$$
\check{p}_{\text{rms}} = \sqrt{\text{tr}[\text{tr}_I(\hat{p}\hat{\rho})]^2 - \text{tr}[\text{tr}_I(\hat{p}\hat{\rho})^2]}, \tag{10}
$$

where tr[·] denotes the trace of an operator, tr$_I$[·] denotes the partial trace of an operator over the internal (g, e) state space $\mathcal{H}_I$, and $\hat{p}$ is the momentum operator.

We study the identical pulses. Initially, the Doppler profile is ideally desymmetrized by transferring the population with strictly positive velocity components to the excited state as if they had absorbed $1\hbar k$. Therefore, the numerical simulations do not take into account any limitations of this scheme due to the desymmetrization step. To reach high population-transfer efficiency with the pulses following the desymmetrization pulse, we choose to follow the adiabatic-rapid-passage approach [15,16] with chirped Gaussian laser pulses, with which close to 100% transfer efficiency with robust pulse parameters can be achieved. In this identical-pulse scheme, all pulses after the desymmetrization pulse are identical, with a pulse envelope of the electric field $E(t)$ and instantaneous frequency $\omega_L(t)$ as follows:

$$
E(t) = E_0 e^{-2\ln 2 \frac{t^2}{\tau^2}},
$$
$$
\omega_L(t) = \omega_0 + \alpha t, \tag{11}
$$

where E_0 is the amplitude of the electric field, τ is the pulse duration defined as the full width at half maximum of the intensity profile, and α is the linear chirp rate. Other pulse shapes are possible [17,18], but we choose to implement the simplest possible. The following parameters are used in the simulations: $\tau = 7.07$ ps and $\alpha = 2\pi(250\,\text{GHz/ps})$. The laser spectral width defined as the full width at half maximum of the spectral intensity is $\delta\nu = \frac{\sqrt{4(\ln 2)^2 + \alpha^2\tau^4}}{2\pi\tau} \simeq 1.8$ THz. The peak intensity is $E_0 = 1.5\,\text{kWcm}^{-2}$, which yields a peak Rabi frequency $\Omega_0 = 2\pi(150\,\text{GHz})$, with a dipole strength $d = 1.97$ D [11]. These parameters can be achieved experimentally (see, for example, [19] for femtosecond ultraviolet millijoule class pulses and [20] for terahertz per picosecond chirp-rate production) and have been chosen to keep
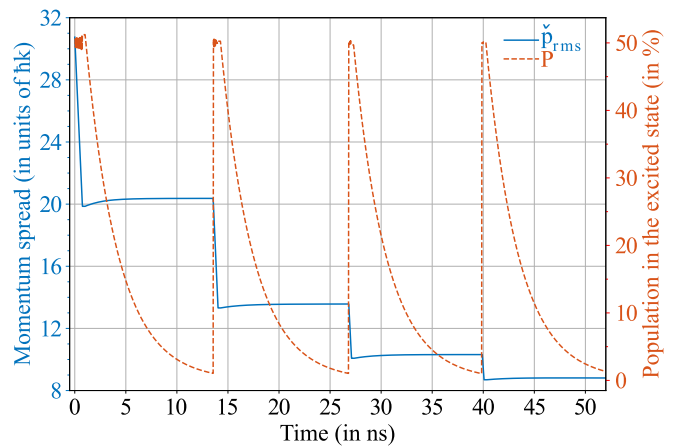

FIG. 5. $\check{p}_{\text{rms}}$ is the momentum rms (solid blue line, left axis) in units of $\hbar k$ simulated as a function of time for a sequence of four identical pulses with an optimized number of pulses. The delay between two consecutive trains is $4\tau_{\text{SE}}$. P is the population in the excited state (dashed red line, right axis) defined as the ratio between the excited state and the sum of the ground and excited states. The sharp falling edges observed in the blue curve has a hyperbolic shape consistent with the red squares displayed in Fig. 3.
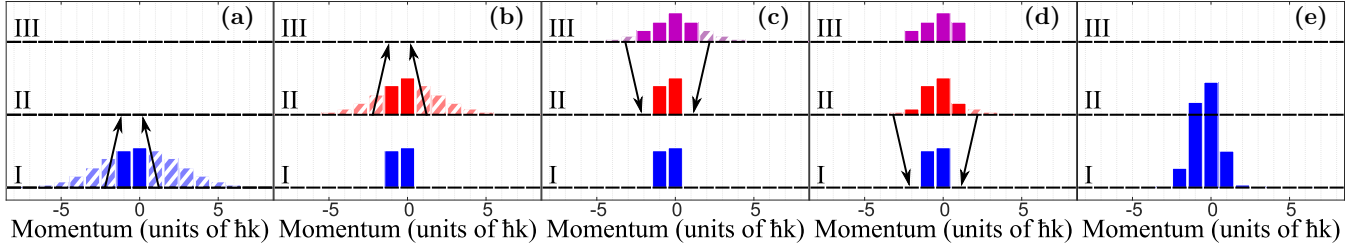
FIG. 6. Illustration of coherent laser cooling with the optimal-transport method for a three-level system on a distribution with an initial momentum rms of $\simeq 5\hbar k$. Colors reflect the electronic internal level. Blue (I) corresponds to the initially populated level. Red (II) and purple (III) are other internal levels. A simple case is when I and III are two distinct levels in the ground- (excited-) state manifold and II is the excited (ground) level. (a) Initial distribution. [(b)–(d)] Intermediate distributions. (e) Distribution after relaxation via spontaneous emission followed by transfer to I. Transfer to I corresponds to the preparation of a single level in the ground-state manifold when I is one of two ground-state levels. When I is one of two excited-state levels, transfer to I corresponds to excitation from the ground-state level II.

the ionization rate in the few percent range. It is also worth mentioning that efficient selective electronic excitation can be achieved with chirped pulses even when the spectral bandwidth is larger than the separation between the different excited states found in a manifold [21]. These parameters are used for all pulses in all trains. In Fig. 3, the result of the numerical simulations ($\check{p}_{rms}$, red squares) shows good quantitative agreement with the evolution predicted by Eq. (2) (p_{rms}, solid blue curve). The minimum reached in the simulation is slightly higher than predicted by Eq. (2), and the number of pulses used to reach this minimum is very close to the predicted one. $\check{p}_{rms}$ is larger than p_{rms}, which we attribute to incomplete population transfer. The population found in the wrong state at the beginning of each pulse is warmed up instead of being cooled. Since the population transfer is very efficient, in the first order approximation once a population is in the wrong state, it stays in the wrong state, and the number of atoms in the wrong states increase with the number of pulses.

To complete this study, we simulate laser cooling with four trains of pulses. Results are presented in Fig. 5. The delay between two consecutive trains is fixed to $4\tau_{SE}$. Each train starts with an ideal desymmetrization step. The number of pulses $M_{m,i}$ in the ith train of pulses is optimized to minimize the momentum rms σ_i at the end of the ith train. In the present case, $M_{m,1} = 26$, $M_{m,2} = 16$, $M_{m,3} = 9$, and $M_{m,4} = 6$. At the end of the fourth train, the rms reaches $8.6\hbar k$, representing a gain of only $1.5\hbar k$ with respect to $\sigma_{m,3}$. Therefore, in this particular case, this scheme becomes less efficient than traditional laser cooling at the end of the third train of pulses.

Finally, we propose that the optimal-transport coherent-laser-cooling scheme can be extended to N-level systems considering levels that are part of only two manifolds and a system initially prepared in a single state of one of the two manifolds. Figure 6 illustrates how optimal transport can be extended to the three-level case. With this method, Eq. (4) can be generalized to the N-level case as described for $M \geqslant 1$ by Eq. (A4) given in Appendix. For a Maxwell-Boltzmann distribution with an initial momentum rms $\tilde{p}_{rms,0}$ large compared to $N\hbar k$ and no particle initially in any of the other states, the population in the class of momentum with $n\hbar k$ when all N

levels are used is written as

$$\sum_{z=0}^{N-1} \rho_0(Nn+z) \simeq \frac{N}{\tilde{p}_{rms,0}\sqrt{2\pi}} e^{-\frac{N^2(n\hbar k)^2}{2\tilde{p}_{rms,0}^2}},$$

which corresponds to a Maxwell-Boltzmann distribution with a momentum rms divided by a factor N compared to the initial
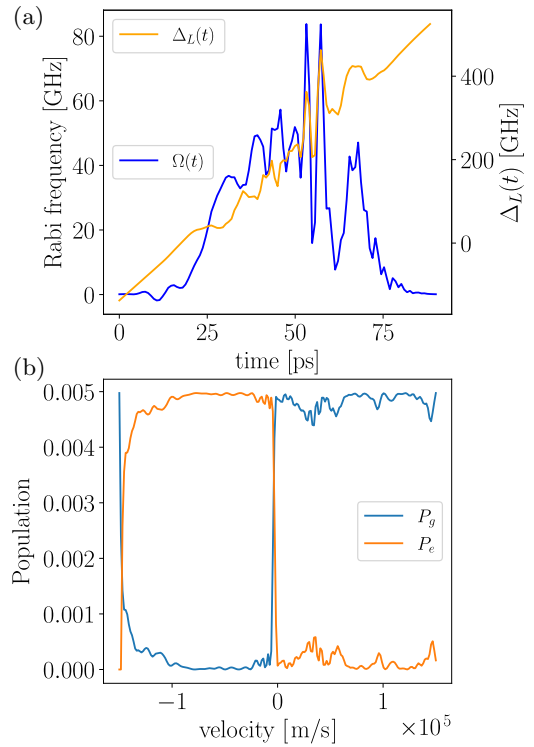

FIG. 7. Desymmetrization step for a two-level system with properties similar to positronium. (a) Instantaneous Rabi frequency $\Omega(t)$ and frequency detuning $\Delta_L(t)$. (b) Population in the ground (P_g) and excited (P_e) states at the end of the desymmetrization pulse displayed in (a). The initial population is in the ground state and is equally spread across 201 classes of velocity spanning the -1.5 to 1.5×10^5 ms^{-1} range. Thus, the highest population in one class of velocity is 0.005. The percentage of atoms in the wrong state at the end of the desymmetrization pulse is 6%.

one. The precise efficiency of such multilevel coherent laser cooling goes beyond the scope of the present study. However, we note that the complexity of the required pulse shaping and the time needed to prepare the initial distribution with all particles in a single level of a manifold will most likely limit the interest of such an extension.

As a final note, the fully optimized shaping of a desymmetrization pulse is outside the scope of the present work but can be approached by optimization using, for example, the Krotov algorithm [9]. An example of such a pulse is given in Fig. 7.

VI. CONCLUSION

In conclusion, our study introduced a laser-cooling scheme based on trains of ultrashort pulses extending coherent laser cooling to broad linewidth transitions. This technique is particularly relevant for distributions with a large initial momentum spread and shows that it is possible to remove several $\hbar k$ per spontaneous emission lifetime. It is particularly important to optimize the time it takes to compress the momentum-spread compression in particular in view of forming a Bose-Einstein condensate [22,23] to generate coherent γ-ray emission by coherence transfer from positronium [24] or radioactive elements [25]. We derived analytical formulas predicting the evolution of the momentum distribution rms as a function of the number of pulses in the train for two different schemes for population manipulation. The identical pulses makes use of an optimal number of identical pulses. Optimal transport allows us to realize the maximum of momentum rms reduction without entropy dissipation (a factor of 2 for a two-level system). We found that in the case studied here, a delay of $4\tau_{\mathrm{SE}}$ between two consecutive trains of pulses allows us to optimize the cooling process. These results were confirmed by realistic numerical simulations. For systems with more than two internal levels, it is, in principle, possible to further increase the efficiency of this laser-cooling scheme, which could be particularly interesting for molecule laser cooling.

APPENDIX

$$p_{\mathrm{rms},0} = \sqrt{\sum_n n^2 [\rho_0(n) + \rho_1(n)]}, \tag{A1}$$

$$M_{mc} = \sum_{n>0} n[\rho_0(n) + \rho_0(-n)] + \sum_{n\leqslant 0} \rho_0(n) - \sum_{n>0} n[\rho_1(n) + \rho_1(-n)] + \sum_{n\leqslant 0} \rho_1(n), \tag{A2}$$

$$M_{ms} = 2\sum_{n>0} n\rho_0(-n) + \sum_{n\leqslant 0} \rho_0(n) - 2\sum_{n>0} n\rho_1(-n) + \sum_{n\leqslant 0} \rho_1(n), \tag{A3}$$

$$\tilde{p}_{\mathrm{rms}}^2(M) = \sum_{n=0}^{\lfloor \frac{M}{N-1} \rfloor -1} n^2 \sum_{z=0}^{N-1} \rho_0(Nn+z) + \left\lfloor \frac{M}{N-1} \right\rfloor^2 \sum_{z=0}^{M-\lfloor \frac{M}{N-1} \rfloor(N-1)} \rho_0\left(N\left\lfloor \frac{M}{N-1} \right\rfloor + z\right)$$

$$+ \sum_{n=-\lfloor \frac{M}{N-1} \rfloor}^{-1} n^2 \sum_{z=0}^{N-1} \rho_0(Nn-z) + \left(\left\lfloor \frac{M}{N-1} \right\rfloor + 1\right)^2 \sum_{z=0}^{M-\lfloor \frac{M}{N-1} \rfloor(N-1)} \rho_0\left[-N\left(\left\lfloor \frac{M}{N-1} \right\rfloor + 1\right) - z\right]$$

$$+ \sum_{n\geqslant \lfloor \frac{M}{N-1} \rfloor +1} n^2 \rho_0(n+M) + \sum_{n\leqslant M+1} n^2 \rho_1(n-M) + \sum_{n\leqslant -\lfloor \frac{M}{N-1} \rfloor -2} n^2 \rho_0(n-M+1) + \sum_{n\geqslant -M} n^2 + \rho_1(n+M-1). \tag{A4}$$

[1] W. Ketterle and D. E. Pritchard, Phys. Rev. A **46**, 4051 (1992).

[2] M. Chalony, A. Kastberg, B. Klappauf, and D. Wilkowski, Phys. Rev. Lett. **107**, 243002 (2011).

[3] T. Chanelière, D. Comparat, and H. Lignier, Phys. Rev. A **98**, 063432 (2018).

[4] L. T. Glöggler et al. (AEḡIS Collaboration), Phys. Rev. Lett. **132**, 083402 (2024).

[5] K. Shu, Y. Tajima, R. Uozumi, N. Miyamoto, S. Shiraishi, T. Kobayashi, A. Ishida, K. Yamada, R. W. Gladen, T. Namba, S. Asai, K. Wada, I. Mochizuki, T. Hyodo, K. Ito, K. Michishio, B. E. O'Rourke, N. Oshima, and K. Yoshioka, arXiv:2310.08761.

[6] C. Corder, B. Arnold, and H. Metcalf, Phys. Rev. Lett. **114**, 043002 (2015).

[7] J. P. Bartolotta, M. A. Norcia, J. R. K. Cline, J. K. Thompson, and M. J. Holland, Phys. Rev. A **98**, 023404 (2018).

[8] A. Goepfert, I. Bloch, D. Haubrich, F. Lison, R. Schütze, R. Wynands, and D. Meschede, Phys. Rev. A **56**, R3354 (1997).

[9] M. H. Goerz, D. Basilewitsch, F. Gago-Encinas, M. G. Krauss, K. P. Horn, D. M. Reich, and C. P. Koch, SciPost Phys. **7**, 080 (2019).

[10] I. Bloch, J. Dalibard, and W. Zwerger, Rev. Mod. Phys. **80**, 885 (2008).

[11] C. Zimmer, P. Yzombard, A. Camper, and D. Comparat, Phys. Rev. A **104**, 023106 (2021).

[12] A. J. Metcalf, V. Torres-Company, V. Supradeepa, D. E. Leaird, and A. M. Weiner, Opt. Express **21**, 28029 (2013).

[13] Y. Ma, X. Huang, X. Wang, L. Ji, Y. He, L. Qiu, J. Zhao, Y. Wang, and S. Wu, Opt. Express **28**, 17171 (2020).

[14] D. Manzano, AIP Adv. **10**, 025106 (2020).

[15] J. S. Melinger, S. R. Gandhi, A. Hariharan, J. X. Tull, and W. S. Warren, Phys. Rev. Lett. **68**, 2000 (1992).

[16] V. Malinovsky and J. Krause, Eur. Phys. J. D **14**, 147 (2001).

[17] T. Lu, X. Miao, and H. Metcalf, Phys. Rev. A **75**, 063422 (2007).

[18] S. Guérin, V. Hakobyan, and H. R. Jauslin, Phys. Rev. A **84**, 013423 (2011).

[19] D. Popmintchev, C. Hernández-García, F. Dollar, C. Mancuso, J. A. Pérez-Hernández, M.-C. Chen, A. Hankla, X. Gao, B. Shim, A. L. Gaeta *et al.*, Science **350**, 1225 (2015).

[20] N. Forget, V. Crozatier, and P. Tournois, Appl. Phys. B **109**, 121 (2012).

[21] J. S. Melinger, S. R. Gandhi, A. Hariharan, D. Goswami, and W. S. Warren, J. Chem. Phys. **101**, 6439 (1994).

[22] P. M. Platzman and A. P. Mills, Phys. Rev. B **49**, 454 (1994).

[23] A. Giatzoglou, T. Poomaradee, I. Pohjalainen, S. Rinta-Antila, I. D. Moore, P. M. Walker, L. Marmugi, and F. Renzoni, Nucl. Instrum. Methods Phys. Res., Sect. A **908**, 367 (2018).

[24] H. K. Avetissian, A. K. Avetissian, and G. F. Mkrtchian, Phys. Rev. Lett. **113**, 023904 (2014).

[25] L. Marmugi, P. M. Walker, and F. Renzoni, Phys. Lett. B **777**, 281 (2018).